Journal of
Mechanics of
Materials and Structures

CREEP BUCKLING OF IMPERFECT THIN-WALLED SHALLOW CONCRETE DOMES

Ehab Hamed, Mark A. Bradford and R. Ian Gilbert

Volume 5, Nº 1 January 2010

mathematical sciences publishers

JOURNAL OF MECHANICS OF MATERIALS AND STRUCTURES
Vol. 5, No. 1, 2010

CREEP BUCKLING OF IMPERFECT THIN-WALLED SHALLOW CONCRETE DOMES

EHAB HAMED, MARK A. BRADFORD AND R. IAN GILBERT

The sensitivity of the nonlinear long-term creep behaviour of shallow concrete domes to geometric and material imperfections is investigated in this paper. A nonlinear incremental theoretical model is developed, which accounts for the effects of creep and shrinkage, considers the aging of the concrete material and the variation of the internal stresses and geometry in time, and is applicable for different and nonaxisymmetric imperfection scenarios and loading schemes. The model focuses only on shallow concrete domes, but the modelling concepts and solution techniques can be generated for the creep buckling analysis of different types of thin-walled concrete structures. The field equations are derived using the variational principles of virtual work and using integral-history-type constitutive relations that are based on the principle of superposition. A step-by-step procedure is used for the solution of the governing equations in time, while the solution of the incremental partial differential equations in space is achieved by a separation of variables and expansion into truncated Fourier series in the circumferential direction, along with the use of the multiple shooting method in the meridional direction. Numerical and parametric studies, which highlight the capabilities of the model and which provide insight into the nonlinear long-term behaviour of imperfect shallow concrete domes, are presented. The results show that the structural behaviour and the critical time to cause creep buckling are very sensitive to geometric and material imperfections.

1. Introduction

Like all other engineering structures, concrete structures have a finite design life. While strengthening and upgrading techniques have been recognised and highlighted over the past two decades in order to increase the safety and serviceability of existing structures, an understanding of the long-term behaviour of concrete structures and the development of suitable and reliable theoretical models for their analysis and safety assessment are essential before the application of costly strengthening techniques. These aspects become more critical in thin-walled concrete shells and in shallow spherical shells (domes) in particular, as these structures are vulnerable to the effects of creep and shrinkage, and unfortunately characterized by catastrophic and sudden buckling failures [DPW NSW 1978; Takeuchi et al. 2004; Moncarz et al. 2007].

In general, all concrete shells of revolution should be designed for the combined effects of creep and buckling; yet, considering the shape of the shell, its use in civil engineering applications, the thickness requirements, and the level of applied sustained loads (self-weight, periodic snow, water/earth pressure), it can be observed that the vulnerability of vertical cylindrical or conical concrete shells of revolution (as

Keywords: buckling, concrete, creep, domes, shells.
The work reported in this paper was supported by the Australian Research Council (ARC) through a Discovery Project awarded to the second and third authors.

cooling towers or storage tanks for example) to creep buckling failures is less than the case in shallow concrete domes or other concrete shell roofs, where creep buckling becomes a key-parameter in their design [Zarghamee and Heger 1983; Bockhold and Petryna 2008]. This paper focuses on the influence of creep on the buckling aspects of shallow concrete domes, and particularly, on the sensitivity of the long-term behaviour to structural imperfections. The challenges associated with the modelling, analysis, and quantitative assessment of the creep buckling phenomenon in general concrete structures are also discussed.

Creep effects generally increase the deformations of a concrete structure even at ambient temperatures, and are usually only considered to affect behaviour at the serviceability limit states. However, in thin-walled shallow concrete domes and other structures that may exhibit sudden buckling failures, the deformations caused by creep and other time-dependent effects become more critical and bring the safety of the structure into question. Due to the geometric nonlinearity, creep leads to a reduction of the height of the dome with a consequent increase or modification of the internal stresses. These two effects may interact to produce localised damage, or may lead to a configuration which produces so-called creep buckling, in which the structure loses its stability slowly over time. The dependence of the creep strains on the level of stresses, their interaction with nonmechanical shrinkage and thermal strains, the aging of the concrete material, and the effects of structural imperfections that cannot be avoided in practice, make accurate prediction of the nonlinear behaviour of concrete domes a challenging and difficult task.

The buckling behaviour of elastic domes has been intensively studied; see for example [Reissner 1946; Sheinman 1981; Błachut and Galletly 1990; 1995; Muc 1992; Teng and Lou 1997; Teng and Song 2001; Hong and Teng 2002; Wunderlich and Albertin 2002; Grigolyuk and Lopanitsyn 2003; Teng and Hong 2006; Marcinowski 2007]. These studies revealed the main aspects that characterize the buckling behaviour of domes, which include snap-through behaviour, the sensitivity of the dome to geometric imperfections, the existence of asymmetric bifurcation points even under axisymmetric loads, and the mode switching and mode interaction in the post buckling deformations. These studies also provided the required theoretical models and numerical tools for the nonlinear analysis of general domes under arbitrary loadings. However, all the aforementioned studies focused only on the nonlinear instantaneous behaviour of domes made of an elastic material, while the nonlinear long-term effects which characterize concrete domes were not investigated.

Only a few research works have focused on the buckling behaviour of concrete domes in general, and a much smaller number of these have focused on the influence of creep on their nonlinear behaviour. In terms of experimental findings, which reveal the importance of considering the long-term effects, Litle et al. [1970] investigated the buckling behaviour of two spherical reinforced mortar domes. It was found that the experimental buckling pressures were only approximately 40% of the classical theoretical value, due to cracking, geometric imperfections, and long-term effects. Vandepitte and Lagae [1986] indicated that the buckling analysis of concrete domes must account for long-term effects and that classical buckling formulae provide much higher buckling pressures than was observed in their experimental work. Based on a decade of a comprehensive experimental work, they observed that creep caused a significant reduction (about 67%) in the buckling pressure. Thus, under sustained loading, a dome may collapse over time under only 33% of its buckling pressure.

In terms of theoretical models, Teng and Rotter [1992] developed a general finite element model for the geometrically and materially nonlinear analysis of reinforced concrete shells of revolution. However,

the long-term effects of the concrete were not included. Dulácska and Kollár [1995] indicated that various long-term effects can be assessed as multipliers of the classical buckling pressure, but a detailed theoretical or experimental basis that supports the proposed factored buckling pressure was not found. Zarghamee and Heger [1983] presented a design procedure for determining the buckling pressure of concrete domes, based on a computer program that was developed by Bushnell [1976] and uses the rate-of-creep method (the Dischinger method). However, the rate-of-creep method is more suitable for materials that exhibit almost linear or bilinear creep behaviour in time. The rate of creep of the concrete material approaches zero as time increases. Hence, when this method is applied for the buckling analysis of concrete structures, where creep causes a significant variation of the internal stresses in time or when the structure is gradually loaded, it may lead to erroneous results because of its inability to accurately asses the creep caused by loads that are applied at older ages [Bažant 1988; Gilbert 1988]. Therefore, a model that is able to account for these effects needs to be implemented in the creep buckling analysis of concrete domes.

The effects of creep and shrinkage on the behaviour of concrete structures have been widely studied and reported [Bažant 1988; Gilbert 1988]. However, very little advanced research appears to have been reported on these effects in concrete shell structures, and in shallow concrete domes in particular. On the other hand, the creep buckling phenomenon of shells and columns made of metals and polymeric composite materials has been studied by many researchers [Hoff 1968; Bushnell 1977; Minahen and Knauss 1993]. Special attention to the creep buckling of circular cylindrical shells was made by [Murakami and Tanaka 1976; Arnold et al. 1989; Miyazaki et al. 1991], and many others. However, in all of these studies, the rate-of-creep method was used, which is of questionable accuracy when applied to concrete structures with stress levels that vary significantly with time.

Similar to the above studies and based on the rate-of-creep method, a few research contributions have been reported on the creep buckling of spherical shells made of metals and other materials. Shi et al. [1970] and Kao [1981] focused only on the nonlinear axisymmetric creep behaviour. It was concluded by Kao [1981] that a creep law that is based on the strain-hardening hypotheses (where the creep rate is a function of the accumulated creep strain) provides more accurate results than the time-hardening hypotheses (where the creep rate is a function of time elapsed since creep started) (also see [Arbabi-Kanjoori and Leonard 1979]). Yet, these two models cannot be used separately for the geometrically nonlinear analysis of concrete structures, because they significantly underestimate the additional creep due to stress changes [Bažant 1987]. Xirouchakis and Jones [1980] studied the full nonlinear creep behaviour considering an imperfection shape according to the classical axisymmetric buckling mode only. Miyazaki [1986] developed a finite element procedure for the creep buckling analysis of spherical shells of revolution considering the bifurcation behaviour, but without considering the effects of imperfections. Huang [1965] used the Volterra integral constitutive relation, which is applicable for aging materials, for the analysis of clamped shallow spherical shells. However, the model is limited to the axisymmetric analysis of shells made of polymethyl-methacrylate with uniform thickness and clamped edges.

It can be seen that most of the existing research contributions have focused on domes made of metals and other materials, where the use of the rate-of-creep method (strain hardening or time hardening) is justified. These existing studies are also limited to specific geometry and boundary conditions, and cover only a small range of imperfection scenarios that can exist in concrete domes. The main objective of this paper is to provide insight into the creep buckling behaviour of thin-walled imperfect shallow concrete

domes, in order to enhance their effective design and safe use, and to contribute to the establishment of a foundation of theoretical knowledge required for nonlinear long-term analysis of concrete structures. Another goal of the paper is to present and to study a different aspect of the influence of creep beyond the service limit state of concrete structures. Studying the behaviour of shallow concrete domes can best contribute to this, because along with other roof shells, these structures are more prone to creep buckling failures than other concrete shells of revolution. A general theoretical model that accounts for the nonlinear creep and shrinkage effects using a history integral-type analysis rather than a rate-of-creep analysis, is developed. The model accounts for the aging of the concrete, different geometry configurations and boundary conditions, and different axisymmetric and nonaxisymmetric loading and imperfection shapes. A study of the creep and shrinkage effects on the geometrically linear behaviour of shallow concrete domes under service loads was conducted by the authors [Hamed et al. 2009b]. The effects of creep and shrinkage on the geometrically nonlinear behaviour were also studied [Hamed et al. 2008; 2009a; 2010] but considering axisymmetric behaviour only and without including the effects of imperfections.

The variational principle of virtual work is used to derive the field equations and the boundary conditions for the problem. Due to the use of an implicit integral-type constitutive relation, a time incremental superposition approach is invoked to formulate the time-dependent governing equations, where the creep and shrinkage strains are treated as initial strains and kept constant with each time step interval [Bažant 1988]. The time integration scheme utilises a slightly variable time step, to account for the decrease of the creep rate, and to account for the rapid change of the structural response prior to buckling. It is assumed that the dome behaves quasistatically, that is, the effects of inertia forces are neglected. Finally, as a first step, and in order to focus on and clarify the stability characteristics of the dome, the analysis is conducted in the framework of linear elasticity. Numerical and parametric studies are included, which provide some insight into the nonlinear long-term behaviour of imperfect shallow concrete domes through the examination of three different imperfection scenarios. The results highlight the capabilities of the proposed theoretical model, and reveal some aspects of the creep response of these structures.

2. Mathematical formulation

The sign conventions for the coordinates, deformations, loads, and stress resultants of a spherical shallow concrete dome are shown in Figure 1. The variational principle of virtual work is used to derive the nonlinear long-term incremental equilibrium equations along with the boundary conditions, which requires that

$$\delta U + \delta W = 0, \tag{1}$$

where δU and δW are the virtual works of the internal stresses and external loads respectively, and δ is the variational operator. The virtual work of the internal stresses is

$$\delta U = \int_V \left[(\sigma_{\varphi\varphi} + \Delta\sigma_{\varphi\varphi})\delta\Delta\varepsilon_{\varphi\varphi} + (\sigma_{\theta\theta} + \Delta\sigma_{\theta\theta})\delta\Delta\varepsilon_{\theta\theta} + (\sigma_{\varphi\theta} + \Delta\sigma_{\varphi\theta})\delta\Delta\varepsilon_{\varphi\theta} \right] dV, \tag{2}$$

where $\sigma_{\varphi\varphi}$ and $\sigma_{\theta\theta}$ are the stresses in the radial and circumferential directions respectively, $\sigma_{\varphi\theta}$ is the in-plane shear stress, $\varepsilon_{\varphi\varphi}$, $\varepsilon_{\theta\theta}$ and $\varepsilon_{\varphi\theta}$ are the corresponding strains, Δ is the incremental operator, and

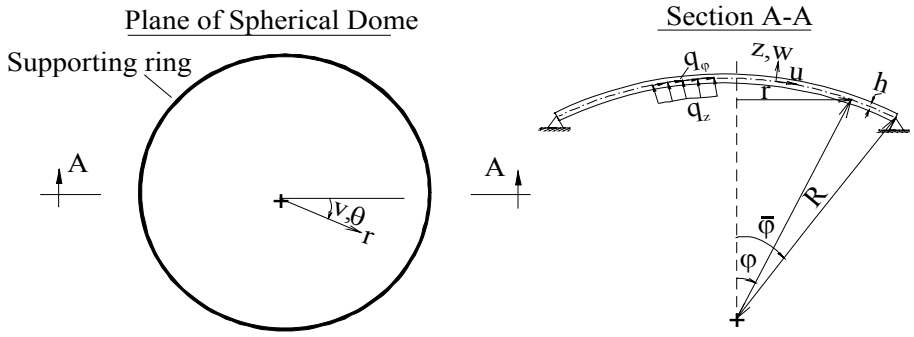

Figure 1. Geometry, loads, and sign conventions.

V is the volume of the dome shell. The virtual work of the external loads is

$$\delta W = -\int_{\theta=0}^{2\pi}\int_{\varphi=0}^{\varphi=\bar{\varphi}} \left[(q_\varphi + \Delta q_\varphi)\delta\Delta u + (q_\theta + \Delta q_\theta)\delta\Delta v + (q_z + \Delta q_z)\delta\Delta w\right] R r(\varphi)\, d\varphi\, d\theta, \tag{3}$$

where u, v, and w are the components of the displacement at the reference surface of the dome shell in the φ, θ, and z directions, respectively (see Figure 1); q_φ, q_θ, and q_z are the corresponding load components, R is the radius of curvature of the spherical dome, and $r(\varphi) = R\sin(\varphi)$ is a horizontal coordinate that runs along the radius of the base parallel circle of the dome (see Figure 1).

2.1. ***Kinematic relations.*** The theoretical model is based on the Kirchhoff–Love hypothesis, for which the strains at any material point (φ, θ, z) are

$$\{\varepsilon(\varphi,\theta,z)\} = \{\bar{\varepsilon}(\varphi,\theta)\} + z\{\kappa(\varphi,\theta)\}, \tag{4}$$

where $\{\varepsilon\} = \{\varepsilon_{\varphi\varphi}, \varepsilon_{\theta\theta}, \varepsilon_{\varphi\theta}\}^T$ is the strain tensor, and $\{\bar{\varepsilon}\} = \{\bar{\varepsilon}_{\varphi\varphi}, \bar{\varepsilon}_{\theta\theta}, \bar{\varepsilon}_{\varphi\theta}\}^T$ and $\{\kappa\} = \{\kappa_{\varphi\varphi}, \kappa_{\theta\theta}, \kappa_{\varphi\theta}\}^T$ are the nonlinear membrane tensor and the change of curvature tensor of the reference surface, respectively.

Based on Donnell's nonlinear shell theory, the incremental strain-displacement relations which account for initial geometric imperfection ($\hat{w}(\varphi,\theta)$), take the following form (for brevity, the notation of the independent coordinates is omitted):

$$\begin{aligned}
\Delta\bar{\varepsilon}_{\varphi\varphi} &= \frac{\Delta u_{,\varphi}}{R} + \frac{\Delta w}{R} + \frac{1}{2}\left(\frac{\Delta w_{,\varphi}}{R}\right)^2 + \frac{w_{,\varphi}\,\Delta w_{,\varphi}}{R^2} + \frac{\hat{w}_{,\varphi}\,\Delta w_{,\varphi}}{R^2},\\
\Delta\bar{\varepsilon}_{\theta\theta} &= \frac{\cos(\varphi)}{r}\Delta u + \frac{\sin(\varphi)}{r}\Delta w + \frac{\Delta v_{,\theta}}{r} + \frac{1}{2}\left(\frac{\Delta w_{,\theta}}{r}\right)^2 + \frac{w_{,\theta}\,\Delta w_{,\theta}}{r^2} + \frac{\hat{w}_{,\theta}\,\Delta w_{,\theta}}{r^2},\\
\Delta\bar{\varepsilon}_{\varphi\theta} &= \frac{\Delta u_{,\theta}}{r} + \frac{\Delta v_{,\varphi}}{R} - \frac{\cos(\varphi)}{r}\Delta v + \frac{\Delta w_{,\theta}\,\Delta w_{,\varphi}}{rR} + \frac{\Delta w_{,\theta}\,(w_{,\varphi}+\hat{w}_{,\varphi})}{rR} + \frac{\Delta w_{,\varphi}\,(w_{,\theta}+\hat{w}_{,\theta})}{rR},\\
\Delta\kappa_{\varphi\varphi} &= -\frac{\Delta w_{,\varphi\varphi}}{R^2},\ \ \Delta\kappa_{\theta\theta} = -\frac{\cos(\varphi)}{rR}\Delta w_{,\varphi} - \frac{1}{r^2}\Delta w_{,\theta\theta},\ \ \Delta\kappa_{\varphi\theta} = \frac{2\cos(\varphi)}{r^2}\Delta w_{,\theta} - \frac{2}{rR}\Delta w_{,\varphi\theta},
\end{aligned} \tag{5}$$

where $(\,)_{,\varphi}$ and $(\,)_{,\theta}$ denote the derivative with respect to the angular and circumferential coordinates respectively. Note that all the deformations that appear without the Δ operator are actually accumulated known deformations from the previous time step. Also note that the strain-displacement relations presented in Equation (5) are valid only for moderate displacements and rather shallow shells.

2.2. ***Equilibrium equations.*** The incremental equilibrium equations are formulated using the variational principle of virtual work, (1)–(3), along with the kinematic relations, (4) and (5), and read

$$
\begin{aligned}
&-(r\,\Delta N_{\varphi\varphi})_{,\varphi} + R\cos(\varphi)\Delta N_{\theta\theta} - (r\,\Delta N_{\varphi\theta})_{,\theta} - r\,R q_{\varphi} = 0,\\
&r\,\Delta N_{\varphi\varphi} + R\sin(\varphi)\Delta N_{\theta\theta} - \Big(\frac{r}{R}\Delta M_{\varphi\varphi}\Big)_{,\varphi\varphi} + \big(\cos(\varphi)\Delta M_{\theta\theta}\big)_{,\varphi} - \Big(\frac{R}{r}\Delta M_{\theta\theta}\Big)_{,\theta\theta}\\
&-\Big(\frac{2R}{r}\cos(\varphi)\Delta M_{\varphi\theta}\Big)_{,\theta} - (2\Delta M_{\varphi\theta})_{,\varphi\theta} - \Big(\frac{r}{R}(N_{\varphi\varphi}+\Delta N_{\varphi\varphi})\Delta w_{,\varphi}\Big)_{,\varphi} - \Big(\frac{r}{R}\Delta N_{\varphi\varphi}(w_{,\varphi}+\hat{w}_{,\varphi})\Big)_{,\varphi}\\
&\quad - \Big(\frac{R}{r}(N_{\theta\theta}+\Delta N_{\theta\theta})\Delta w_{,\theta}\Big)_{,\theta} - \Big(\frac{R}{r}\Delta N_{\theta\theta}(w_{,\theta}+\hat{w}_{,\theta})\Big)_{,\theta} - \big((N_{\varphi\theta}+\Delta N_{\varphi\theta})\Delta w_{,\theta}\big)_{,\varphi}\\
&\quad - \big(\Delta N_{\varphi\theta}(w_{,\theta}+\hat{w}_{,\theta})\big)_{,\varphi} - \big((N_{\varphi\theta}+\Delta N_{\varphi\theta})\Delta w_{,\varphi}\big)_{,\theta} - \big(\Delta N_{\varphi\theta}(w_{,\varphi}+\hat{w}_{,\varphi})\big)_{,\theta} - q_z r R = 0,\\
&-(R\,\Delta N_{\theta\theta})_{,\theta} - (r\,\Delta N_{\varphi\theta})_{,\varphi} - R\cos(\varphi)\Delta N_{\varphi\theta} - r\,R q_{\theta} = 0,
\end{aligned}
\tag{6}
$$

with $N_{\varphi\varphi}$, $N_{\theta\theta}$, and $N_{\varphi\theta}$ being the radial, circumferential, and shear forces, respectively; and $M_{\varphi\varphi}$, $M_{\theta\theta}$, and $M_{\varphi\theta}$ are the bending moments.

The boundary conditions, which result from the variational calculus, are

$$
\begin{aligned}
&kr N_{\varphi\varphi} = \bar{N}_{\varphi\varphi} \quad \text{or} \quad u = \bar{u},\\
&kr N_{\varphi\theta} = \bar{N}_{\varphi\theta} \quad \text{or} \quad v = \bar{v},\\
&k\Big[\frac{r}{R}(N_{\varphi\varphi}+\Delta N_{\varphi\varphi})\Delta w_{,\varphi} + \frac{r}{R}\Delta N_{\varphi\varphi}(w_{,\varphi}+\hat{w}_{,\varphi}) + \Big(\frac{r}{R}M_{\varphi\varphi}\Big)_{,\varphi}\\
&\qquad - \cos(\varphi)M_{\theta\theta} + (2M_{\theta\theta})_{,\theta} + (N_{\varphi\theta}+\Delta N_{\varphi\theta})\Delta w_{,\theta} + \Delta N_{\varphi\theta}(w_{,\theta}+\hat{w}_{,\theta})\Big] = \bar{P}_z \quad \text{or} \quad w = \bar{w},\\
&-k\frac{r}{R}M_{\varphi\varphi} = \bar{M}_{\varphi\varphi} \quad \text{or} \quad w_{,\varphi} = \bar{w}_{,\varphi},
\end{aligned}
\tag{7}
$$

where $\bar{N}_{\varphi\varphi}$, $\bar{N}_{\varphi\theta}$, $\bar{P}_z$, and $\bar{M}_{\varphi\varphi}$ are external loads and bending moments at the boundaries; the over-bar designates prescribed deformations; $k = 1$ where $\varphi = \bar{\varphi}$ and $k = -1$ where $\varphi = 0$.

2.3. ***Constitutive relations.*** The principle of superposition is adopted here for describing the time-dependent stress-strain relations, which accounts for the aging of the concrete material, as well as, the variation of the internal stresses and the dome's shape in time [Bažant 1988; Gilbert 1988]. Although this approach is more applicable for linear stress-strain relations; in practice, most thin-walled shallow concrete domes are designed to stay in the linear range, and in many cases buckling may occur under this level of stresses where the principle of superposition holds [Zarghamee and Heger 1983]. The study of the creep effects at the materially linear level provides a theoretical basis and a basic understanding for developing more advanced theoretical models that account for the material nonlinearity.

The history integral-type constitutive relations take the form

$$
\{\varepsilon(t)\} = \int_{t_o}^{t} J(t,t')[B]\,d\{\sigma(t')\} + \{\varepsilon_{\mathrm{sh}}(t)\} \quad \text{or} \quad \{\sigma(t)\} = \int_{t_o}^{t} \bar{R}(t,t')[B]^{-1}\big(d\{\varepsilon(t')\} - d\{\varepsilon_{\mathrm{sh}}(t')\}\big), \tag{8}
$$

where $J(t,t')$ is the compliance or creep function, $\bar{R}(t,t')$ is the relaxation function, $\varepsilon_{\mathrm{sh}}$ is the shrinkage strain, t_o corresponds to the time at first loading/deforming, and $[B]$ is an elastic matrix that takes the

form

$$[B] = \begin{pmatrix} 1 & -\nu & 0 \\ -\nu & 1 & 0 \\ 0 & 0 & \dfrac{1-\nu}{2} \end{pmatrix}, \tag{9}$$

where ν is Poisson's ratio, which is assumed to be constant with time [Bažant 1988]. It is also assumed that the creep/relaxation function under biaxial loading is similar to the one obtained under uniaxial loading, while the matrix $[B]$ introduces the Poisson's effect [Buyukozturk and Shareef 1985; Bažant 1988].

The governing equations in terms of the unknown deformations (u, v, w) that are based on Equation (8) suffer from the existence of implicit integral expressions, which introduce a major difficulty in their solution. Because of this, an incremental procedure that was first developed by Bažant [1972] for the geometrically linear analysis of concrete structures is adopted and further extended here to the geometrically nonlinear analysis (also see [Bažant 1988]). According to the incremental approach, the time t is subdivided into n_t discrete times with $\Delta t_i = t_i - t_{i-1}$ $(i = 1, 2, \ldots, n_t)$. Using the trapezoidal numerical integral rule, the integral constitutive relation presented in (8) is approximated as

$$\{\varepsilon(t_i)\} = J(t_i, t_o)[B]\{\sigma(t_o)\} + \{\varepsilon_{\mathrm{sh}}(t_i)\} + \sum_{s=1}^{i}\left(\frac{J(t_i, t_s) + J(t_i, t_{s-1})}{2}\right)[B]\{\sigma(t_s) - \sigma(t_{s-1})\}. \tag{10}$$

Using the same procedure for the strain at t_{i-1}, the following incremental stress-strain relations are obtained, which present a quasistatic relation with a modulus E'' along with a prescribed incremental strain $\Delta\varepsilon''$ that introduces the effects of the creep and shrinkage into the system

$$\{\Delta\varepsilon(t_i)\} = \frac{1}{E''(t_i)}[B]\{\Delta\sigma(t_i)\} + \{\Delta\varepsilon''(t_i)\} \quad \text{or} \quad \{\Delta\sigma(t_i)\} = E''(t_i)[B]^{-1}\{\Delta\varepsilon(t_i) - \Delta\varepsilon''(t_i)\}, \tag{11}$$

and correspondingly

$$\{\Delta N(t_i)\} = E''(t_i)h[B]^{-1}\{\Delta\bar{\varepsilon}(t_i) - \Delta\tilde{\varepsilon}(t_i)\}, \quad \{\Delta M(t_i)\} = E''(t_i)\frac{h^3}{12}[B]^{-1}\{\Delta\kappa(t_i) - \Delta\tilde{\kappa}(t_i)\}, \tag{12}$$

where $\{\Delta N\} = \{\Delta N_{\varphi\varphi}, \Delta N_{\theta\theta}, \Delta N_{\varphi\theta}\}^T$ and $\{\Delta M\} = \{\Delta M_{\varphi\varphi}, \Delta M_{\theta\theta}, \Delta M_{\varphi\theta}\}^T$, and h is the thickness of the dome shell.

The incremental modulus and incremental strains caused by creep and shrinkage are

$$E''(t_i) = \frac{2}{J(t_i, t_i) + J(t_i, t_{i-1})}, \tag{13}$$

$$\begin{aligned}\{\Delta\tilde{\varepsilon}(t_i)\} = {} & \big(J(t_i, t_o) - J(t_{i-1}, t_o)\big)[B]\frac{\{N(t_o)\}}{h} + \{\varepsilon_{\mathrm{sh}}(t_i) - \varepsilon_{\mathrm{sh}}(t_{i-1})\} \\ & + \sum_{s=1}^{i-1}\left(\frac{J(t_i, t_s) + J(t_i, t_{s-1})}{2} - \frac{J(t_{i-1}, t_s) + J(t_{i-1}, t_{s-1})}{2}\right)[B]\frac{\{N(t_s) - N(t_{s-1})\}}{h},\end{aligned} \tag{14}$$

$$\begin{aligned}\{\Delta\tilde{\kappa}(t_i)\} = {} & \big(J(t_i, t_o) - J(t_{i-1}, t_o)\big)[B]\frac{\{M(t_o)\}12}{h^3} \\ & + \sum_{s=1}^{i-1}\left(\frac{J(t_i, t_s) + J(t_i, t_{s-1})}{2} - \frac{J(t_{i-1}, t_s) + J(t_{i-1}, t_{s-1})}{2}\right)[B]\{M(t_s) - M(t_{s-1})\}\frac{12}{h^3}.\end{aligned} \tag{15}$$

2.4. ***Governing equations.*** The incremental governing equations are formulated by substitution of the incremental constitutive relations, (12)–(15), into the equilibrium equations, (6), noting that terms that include uncoupled functions from the initial state (or previous increment) vanish since they are in equilibrium, and that terms of higher order product of the incremental displacement may be neglected due to the use of sufficiently small increments in time. The incremental governing equations are written in terms of the unknown deformations:

$$\psi_p(\Delta u, \Delta v, \Delta w) = 0, \qquad p = 1, 2, 3, \tag{16}$$

where ψ_p consists of differential operators. For brevity, the explicit form of these equations is not presented here.

This incremental formulation, which is based on the history integral constitutive relation, requires that at each time increment all the preceding values of the stresses and strains that are represented in terms of prescribed strains ($\Delta\tilde{\varepsilon}_{\varphi\varphi}$, $\Delta\tilde{\varepsilon}_{\theta\theta}$, $\Delta\tilde{\kappa}_{\varphi\varphi}$, and $\Delta\tilde{\kappa}_{\theta\theta}$) in (12) must be stored by means of (14) and (15). Despite this, the method is preferred over the incremental differential-type formulation because in the nonlinear case studied here, where the internal stresses may significantly vary with time, the conversion of the constitutive equation of an integral type to one of a differential type using a series expansion (a Dirichlet series for example [Bažant 1988]) is required at each time increment. This procedure is difficult, consuming in computational effort, and in essence only provides an approximation to the compliance function. Moreover, in many cases the use of differential type constitutive relations based on Kelvin or Maxwell chains violate basic thermodynamics laws, where the spring moduli and dashpot viscosities become negative [Bažant and Chern 1984].

2.5. ***Time dependent parameters.*** In general, the creep and shrinkage characteristics of concrete are highly variable and are never known exactly. There are many theoretical models which aim to predict the time-dependent behaviour of concrete [Bažant 1988; Gilbert 1988]. In this paper, the influences of creep and shrinkage are introduced based on the well-known and commonly used recommendations of [ACI 1982]. The shrinkage strain includes the influences of the drying, autogenous, and carbonation shrinkage. It is assumed here that the shrinkage strain is axisymmetric, and uniform along the meridian of the dome and through its thickness, and takes the following algebraic empirical form:

$$\varepsilon_{\mathrm{sh}}(\varphi, \theta, z, t) = \varepsilon_{\mathrm{sh}}(t) = \frac{t^{\beta}}{f + t^{\beta}} \varepsilon_{\mathrm{sh}}^{u}, \tag{17}$$

where β and f are parameters that control the magnitude of the shrinkage strain, and $\varepsilon_{\mathrm{sh}}^{u}$ is the final shrinkage strain, at time infinity.

[ACI 1982] recommends the following expression for the creep or compliance function, which includes the effects of basic and drying creep:

$$J(t, t') = \frac{1 + \phi(t, t')}{E(t')}, \tag{18}$$

where $\phi(t, t')$ is the creep coefficient and is evaluated as follows:

$$\phi(t, t') = \left[\frac{(t - t')^{\lambda}}{d + (t - t')^{\lambda}} \right] \phi_u(t'). \tag{19}$$

λ and d are wide-range parameters that control the creep coefficient, and the time t and the age of loading t' are measured in days. $\phi_u(t')$, which depends on the age of loading, takes the following form for moist cured concrete:

$$\phi_u(t') = 1.25 \times t'^{(-0.118)} \phi(\infty, 7). \tag{20}$$

$\phi(\infty, 7)$ is the final creep coefficient at time infinity for a load first applied at age 7 days [ACI 1982; AS 3600 2001].

The modulus of elasticity takes the following form [AS 3600 2001]:

$$E(t') = 0.043\rho^{1.5}\sqrt{f_c(t')} \quad \text{(in MPa)}, \tag{21}$$

where ρ is the concrete mass density (in kg/m^3) and f_c is the time dependent characteristic compressive strength of the concrete (in MPa), which is given by [ACI 1982]

$$f_c(t') = \frac{t'}{\alpha + \gamma\, t'} f_c^{28}, \tag{22}$$

where f_c^{28} is the characteristic compressive strength at 28 days, and α and γ are constants. The above expressions show that the compliance function (18) depends on the age of loading and introduces the effect of aging into the system.

3. Solution procedure

The set of incremental partial differential equations, (16), and their boundary conditions, (7), are reduced to a set of ordinary differential equations by a separation of variables and expansion into truncated Fourier series [Hong and Teng 2002; Sheinman and Jabareen 2005]:

$$\{\Delta u(\varphi, \theta), \Delta v(\varphi, \theta), \Delta w(\varphi, \theta)\} = \sum_{m=0}^{2F} \{\Delta u_m(\varphi), \Delta v_m(\varphi), \Delta w_m(\varphi)\} g_m(\theta), \tag{23}$$

where $F = (F_u, F_v, \text{or } F_w)$ is the number of terms in the relevant Fourier series. The solution of the initial state (or previous increment), the geometric imperfection, the external load (which can be of any shape and not necessarily axisymmetric), and the incremental initial strains at each time increment that results from creep and shrinkage, take this form:

$$\{u(\varphi, \theta), v(\varphi, \theta), w(\varphi, \theta)\} = \sum_{m=0}^{2F} \{u_m(\varphi), v_m(\varphi), w_m(\varphi)\} g_m(\theta), \tag{24}$$

$$\hat{w}(\varphi, \theta) = \sum_{m=0}^{2F_w} \hat{w}_m(\varphi) g_m(\theta), \tag{25}$$

$$\{q_\varphi(\varphi, \theta), q_\theta(\varphi, \theta), q_z(\varphi, \theta)\} = \sum_{m=0}^{2Fq} \{q_{\varphi m}(\varphi), q_{\theta m}(\varphi), q_{zm}(\varphi)\} g_m(\theta), \tag{26}$$

$$\{\Delta\tilde{\varepsilon}(\varphi, \theta)\} = \sum_{m=0}^{2Fc} \{\Delta\tilde{\varepsilon}_m(\varphi)\} g_m(\theta), \tag{27}$$

$$\{\Delta\tilde{\kappa}(\varphi,\theta)\} = \sum_{m=0}^{2Fc} \{\Delta\tilde{\kappa}_m(\varphi)\} g_m(\theta), \tag{28}$$

where $Fq = (Fq_\varphi,\ Fq_\theta$, or $Fq_z)$, and $Fc = (Fc_{\varphi\varphi},\ Fc_{\varphi\theta}$, or $Fc_{\theta\theta})$ are the number of terms in the relevant Fourier series. The functions $g_m(\theta)$ are

$$g_m(\theta) = \begin{cases} \cos(nm\theta), & m = 0, 1, \ldots, F, \\ \sin[n(m-F)\theta], & m = F+1, \ldots, 2F, \end{cases} \tag{29}$$

where n is the characteristic circumferential wave number.

Minimization of the errors due to the truncated Fourier series by the Galerkin procedure with trigonometric weighting functions yields the nonlinear ordinary differential equations

$$\Psi_p^m(\varphi) = \oint \psi_p(u, v, w) g_m(\theta)\, d\theta \qquad m = 0, 1, \ldots, 2F, \quad p = 1, 2, 3. \tag{30}$$

As $r \to 0$, the solution of the equations becomes singular at the pole (see (6)). In order to prevent this singularity, the strains and change of curvature must remain finite as $r \to 0$. In other words, $\lim_{r\to 0}\{\Delta\bar{\varepsilon}\}$ and $\lim_{r\to 0}\{\Delta\kappa\}$ must be finite. Following Gould [1988], and noting that $n \geq 4$ based on Donnell's theory, these requirements, which are treated by the aid of l'Hospital's rule, yields the following boundary conditions at the pole:

For $m = 0$ (axisymmetric):

$$u = 0, \qquad v = 0, \qquad w_{,\varphi} = 0, \tag{31}$$

$$\frac{r}{R}(N_{\varphi\varphi} + \Delta N_{\varphi\varphi})\Delta w_{,\varphi} + \frac{r}{R}\Delta N_{\varphi\varphi}(w_{,\varphi} + \hat{w}_{,\varphi}) + \left(\frac{r}{R}M_{\varphi\varphi}\right)_{,\varphi} - \cos(\varphi)M_{\theta\theta} + (2M_{\theta\theta})_{,\theta} + (N_{\varphi\theta} + \Delta N_{\varphi\theta})\Delta w_{,\theta} + \Delta N_{\varphi\theta}(w_{,\theta} + \hat{w}_{,\theta}) = 0. \tag{32}$$

For $m \geq 1$ (nonaxisymmetric):

$$u = 0, \qquad v = 0, \qquad w = 0, \qquad w_{,\varphi} = 0. \tag{33}$$

Equations (31)–(33) impose the boundary conditions at the dome's pole only, while the actual boundary conditions at the edge of the dome are defined or generated via (7).

The solution of the coupled governing equations and the boundary conditions in the meridional direction is conducted via the multiple shooting numerical method [Stoer and Bulirsch 2002]. In order to account for the possible bifurcation and mode-switching (secondary bifurcation) behaviours of the dome, the load-disturbance method is used. In this method, very small nonaxisymmetric loads in selected harmonics are added to the axisymmetric loads to guide the structure into the new equilibrium mode (see [Teng and Hong 2006] for more details). The analysis is conducted up to a certain time (the ultimate time) where the rate of deformation of the system begins to increase rapidly and becomes infinite or when the deformations exceed prescribed limits [Murakami and Tanaka 1976; Miyazaki 1986]. The development of bifurcation points through the time response, which may or may not result in instantaneous loss of load carrying capacity [Obrecht 1977], is accounted for as an automatic outcome of the full nonlinear analysis combined with the load disturbance method, rather than by performing a perturbation analysis. In order to account for the rapid increase of the deformations rate at certain points, to consider the fact that the

rate of creep is higher at the early ages of loading, and to account for gradually increasing loadings, the time step was kept relatively small and almost constant through the entire analysis. However, at certain points or time domains, a reduction of the time step is required, and in other cases, an increase is allowed. In this paper, user intervention was used when necessary. The appropriate time step for a given loading is selected so that the difference between the ultimate times based on the selected time step and one-half of this step is of minor significance [Kao 1981].

4. Numerical study

The geometry of the examined dome, which is loaded by an axisymmetric vertical load, is given in Figure 2a. The boundary conditions at the edge are $u = v = w = M_{\varphi\varphi} = 0$, which are derived via (7), while the conditions at the pole are given by (31)–(33). The characteristic compressive strength and modulus of elasticity of the concrete (N32) are taken as 32 MPa and 28.6 GPa respectively [AS 3600 2001], with a Poisson's ratio of 0.15, and a mass density of $\rho = 2400\,\text{kg/m}^3$. Note that the mass density is given for the determination of the time-dependent modulus of elasticity through (21) and for the determination of the dead load, but not for any dynamic effects. Based on the recommendations of [ACI 1982; Gilbert 1988], the following values are adopted for the parameters that control the long-term behaviour: $\beta = 1$, $f = 35$, $\varepsilon^u_{\text{sh}} = -780\,\mu\varepsilon$, $\lambda = 0.6$, $d = 10$ days, $\phi(\infty, 7) = 2.35$, $\alpha = 4$, and $\gamma = 0.85$. Note that the radial and perpendicular components of the vertical load are considered in the analysis, which become nonuniform and depend upon the radial coordinate.

4.1. ***Short-term behaviour.*** For reference, the short-term behaviour of the perfect shallow dome is studied first in Figure 2b and Figure 2c using the characteristic modulus of elasticity. The governing equations for the short-term analysis can be easily generated from (6) by dropping all the terms that are related to the response at the previous increment, and by dropping the Δ operator. These equations are not incremental ones, in which the solution at each load level can be obtained by a straightforward procedure using the arc-length continuation technique [Sundararajan and Noah 1997]. The normalized equilibrium path, Figure 2b, shows that the shallow dome is characterized by a limit-point type of behaviour with no bifurcation point observed at the examined range of displacements. Yet, examining a wider range of displacements

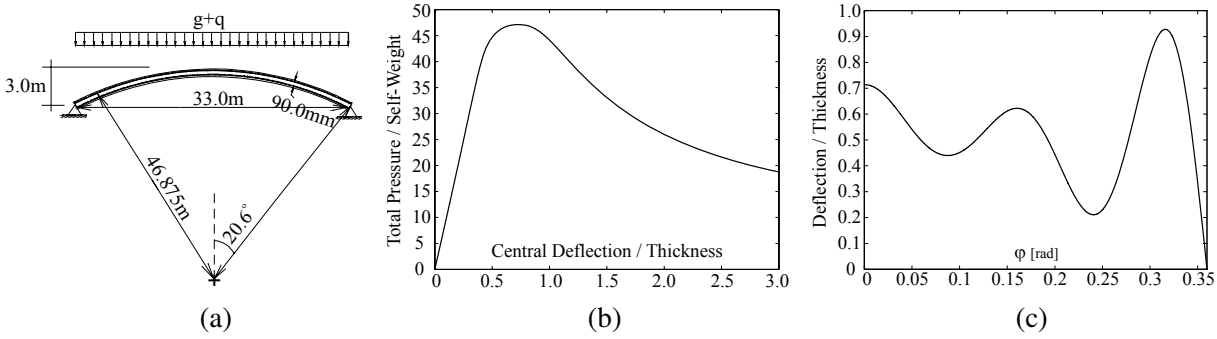

Figure 2. Numerical example: (a) geometry of a shallow dome; (b) short-term loading equilibrium path; (c) axisymmetric buckling mode.

may reveal primary and secondary bifurcation points in the postbuckling range. Nevertheless, the postbuckling behaviour of thin walled concrete structures is of little concern in most practical cases because of the brittleness of the concrete material and its very limited ability to undergo a snap-through behaviour, which is associated with dynamic effects and relatively high tensile and compressive strains [Gioncu 1979]. In general, however, perfect shallow domes under axisymmetric loading may exhibit bifurcation points that may appear before or after the limit point. This depends on many parameters including the radius/thickness ratio, the rise/(base diameter) ratio, the boundary conditions, the loading pattern (radial or vertical), and others. In the case studied here, the buckling mode, which is an axisymmetric one, appears in Figure 2c.

As can be seen in Figure 2b, the vertical buckling pressure of the dome equals 47 times its self-weight and the displacement at this point is approximately 0.72 of the thickness of the dome shell. Though the buckling pressure could be very conservative for design purposes, considering the fact that the buckling pressure of imperfect domes could be 50% that of the perfect one [Zarghamee and Heger 1983], and the fact that many concrete domes are subjected to snow loads of the same level of magnitudes as their self-weight, the actual buckling pressure could be as low as 12 times the actual weight of the dome. When the long-term effects of creep and shrinkage are considered, this value could be even much lower as shown subsequently.

Using the classical theoretical value for the buckling pressure [Billington 1982],

$$q_{cr} = C E \left(\frac{h}{R}\right)^2, \tag{34}$$

where $C = 2/\sqrt{3(1-\nu^2)}$, the classical buckling pressure of the dome becomes 57 times its self-weight, which is 19% higher than the one obtained in Figure 2b. The differences are because (34) is based on the linear stability approach that does not account for the nonlinear prebuckling deformations, and because it is appropriate for complete spherical shells and not shallow ones. Also, note that (34) is valid for radial loading only; yet, this result provides a level of verification to the proposed model.

4.2. ***Imperfection scenarios.*** Three different imperfection scenarios that characterize shell structures in general and concrete shells in particular are considered. The first scenario is a case where the imperfection is of the form of the critical buckling mode under axisymmetric loading. Such a scenario is typical for the sensitivity study of shell structures and is recommended by many design codes [Xirouchakis and Jones 1980; Hong and Teng 2008]; thus

$$\hat{w}(\varphi) = \xi h \times \text{buckling mode}, \tag{35}$$

where ξ is the imperfection amplitude, and the buckling mode is plotted in Figure 2c.

The second imperfection scenario, which is almost impossible to be avoided in concrete structures but is also typical to any other structure, results from inaccuracies in the construction process that may lead to small departures from sphericity. A nonaxisymmetric geometric imperfection of the following shape is considered [Kao 1981]:

$$\hat{w}(\varphi, \theta) = \xi h \times \left(1 - \left(\frac{\sin(\varphi)}{\sin(\bar{\varphi})}\right)^2\right)^3 \cos(n\theta). \tag{36}$$

The third imperfection scenario is more unique to concrete domes, and accounts for the potential varying stiffness of the dome in the circumferential direction. Such varying stiffness may result from preloading shrinkage cracks that are parallel to the meridians direction and result from tensioning in the circumferential direction, from a nonuniform thickness of the dome due to construction inaccuracies, or from nonuniform material moduli. The varying stiffness of the dome is introduced here through a symmetrically reduced effective thickness that sinusoidally varies in the circumferential direction (where the combined extensional-bending rigidity is zero) and takes the form

$$h(\theta) = \left(1 - \frac{\xi}{2}\right) h_o + \frac{1}{2}\xi h_o \cos(n\theta). \tag{37}$$

Here, h_o is the nominal (designed) thickness of the dome shell, and ξ corresponds to the reduction factor of the membrane rigidity. Mathematically, this imperfection is also treated using the truncated Fourier series as was shown in Equations (24)–(29). Thus, the thickness profile of the dome becomes

$$h(\varphi, \theta) = \sum_{m=0}^{2F_h} h_m(\varphi) g_m(\theta), \tag{38}$$

where F_h is the number of terms in the Fourier series, and $h_m(\varphi)$ is a constant function in the case studied here in the meridional direction; yet it varies with the corresponding Fourier term (see Equation (37)), while $g_m(\theta)$ introduces the variation in the circumferential direction.

Note that other imperfection scenarios than those examined here may lead to different and even greater drop of the critical load; see for example [Zarghamee and Heger 1983; Błachut and Galletly 1990; 1995]. Yet, this aspect is not investigated here. Nevertheless, using the proposed model, many imperfection scenarios can be studied.

The short-term behaviour of imperfect domes was extensively studied in many research works including the development of theoretical models and numerical tools for their analysis; see for example [Muc 1992; Błachut and Galletly 1990; 1995; Teng and Song 2001; Wunderlich and Albertin 2002]. Therefore, for brevity and clarity, and in order to focus on the goals of this paper, the short-term behaviour of imperfect domes is not presented here.

4.3. ***Long-term behaviour of imperfect dome.*** The long term behaviour under the three imperfection scenarios described above is studied here. In practice, structures are seldom fully loaded at one time, and the loading process usually takes hours and sometimes even days. In this sense, a gradually loading history, which is presented in Figure 3, is considered. For this, the dome is first loaded at age of 7 days by its self-weight, followed by a linearly increasing load at the age of 28 days for a period of one week to reach a magnitude of 50% of its vertical buckling pressure (23.5× self-weight). The load is then held constant. In the following discussion, the time is measured from the age of first loading when the age of the concrete is 7 days, assuming that the structure is fully supported during the first 7 days for curing. The behaviour at $t = 0$ actually corresponds to the instantaneous response of the dome to its self weight without any long-term effects. Because the stresses induced by shrinkage prior loading depends on the supporting scheme before loading and thus on the construction technique, these stresses are ignored before the time of first loading (that is, shrinkage is taken to commence at $t = 0$).

First imperfection scenario: axisymmetric. The variation of the peak perpendicular deflection (observed at $\varphi = 0.316$ rad (18.1°) according to Figure 2c) with time is shown in Figure 4 for the case where the dome is loaded according to Figure 3 and with an axisymmetric imperfection according to the buckling mode as given by Equation (35) and Figure 2c. Different values for the imperfection amplitude ξ are examined; the response with $\xi = 0$ corresponds to the perfect dome. The results reveal that the ultimate time for creep buckling of the perfect dome, where the rate of deformation of the system begins to increase rapidly and becomes infinite, equals 206 days. In reality, at this point the system tends to snap toward a far more stable equilibrium position with a potential development of circumferential nonaxisymmetric deformations. Yet, due to the brittleness and the limited deformability of the concrete material, the dome will generally collapse at the ultimate time once the deformations become large, and does not exhibit a snap through behaviour [Gioncu 1979].

The results presented in Figure 4 show that the ultimate time significantly decreases with the increase of the imperfection amplitude. Thus, thin-walled concrete domes are very sensitive to the existence of geometric imperfections. Despite the use of the load-disturbance method, which allows for the development of bifurcation points and mode switching, no bifurcation point is observed here and the deformation

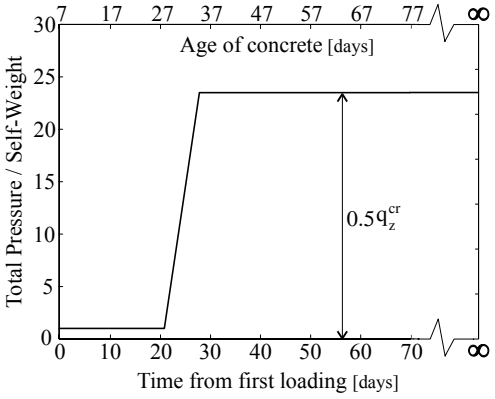

Figure 3. Loading history.

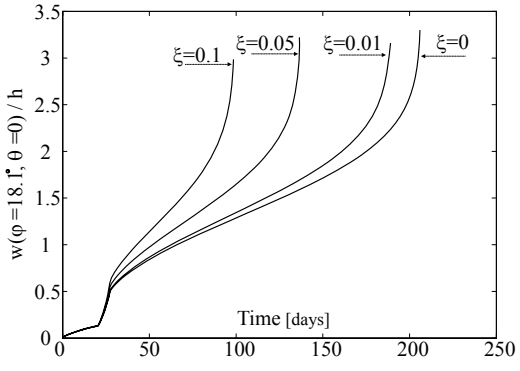

Figure 4. Axisymmetric imperfection: variation in time of peak deflection with different imperfection amplitudes of the buckling mode.

pattern of the dome remains axisymmetric through the entire time domain. The nonlinear sensitivity of the dome to small imperfections indicates the importance of considering these effects through detailed and comprehensive computational models.

Note that with $\xi = 0$, for instance, the rapid increase of the deflection at $t < 50$ days results from the gradual loading and from the nature of creep of the concrete material, which is higher in the first few days after loading. On the other hand, the rapid increase at $t > 180$ days results from the geometric nonlinearity. Comparing the long-term limit deflections that develop at the ultimate time with the short-term limit deflections obtained in Figure 2, it can be seen that the peak deflections develop under a sustained pressure that is half of the vertical buckling pressure are about three times the peak deflections that develop under the full short-term vertical buckling pressure. The normalized peak deflection at $\varphi = 18.1^\circ$ obtained in Figure 2c is 0.93, while the level of normalized deflection in which buckling starts in Figure 4 equals 3.2. Thus, while under short-term loading the structure loses its stability by a combination of large forces and relatively moderate deflections, under sustained load, the structure loses its stability by a combination of moderate forces and relatively large deflections that result from creep and nonlinear coupling as well.

Second imperfection scenario: nonaxisymmetric. The time-dependent behaviour of the dome under the loading history described in Figure 3 and with a nonaxisymmetric imperfection according to Equation (36) is shown in Figure 5 for different imperfection amplitudes. The results show that the amplitude of the nonaxisymmetric imperfection significantly affects the time-dependent behaviour of the dome and should be considered in their design. The response with $\xi = 0.05$ and $\xi = 0.1$ reveals a sudden change in the slope of the curve at certain points, that is, $t = 162$ days and 92 days respectively. These points are considered as critical points, in which the deformation at $\varphi = 18.1^\circ$ sharply increases and becomes affected by nonaxisymmetric deformations. To clarify this, consider Equation (23), which indicates that the total solution is obtained by a summation of the effects of different Fourier harmonics. Figure 6 shows the ratio between the axisymmetric term of the solution w_0 (obtained with $m = 0$) and the total solution. The results show that with $\xi = 0.05$ this ratio is very close to 1 up to $t = 162$ days. At this point, this ratio jumps to 1.12, which reflects a negative contribution of the higher Fourier harmonics on the deflection at $\varphi = 18.1^\circ$ and $\theta = 45^\circ$. A similar behaviour is observed at $t = 92$ days with $\xi = 0.1$.

Because in general, bifurcation or fork points do not necessarily mean a failure of the structure [Obrecht 1977], the effect of these critical points at a different location ($\varphi = 8.0^\circ$ and $\theta = 0$) is examined in Figure 7. The results show that the deflection becomes very large beyond these critical points. Such a level of deflections in concrete structures, which is of the order of 5 to 9 times the thickness of the dome, definitely leads to failure of the structure, and so the critical points observed here can be considered as points that cause creep buckling and failure of the dome. The results presented in Figures 5 and 7 show that in order to identify these *critical* points in a full nonlinear analysis, the deformation-time curve should be examined at multiple points along the surface of the dome. Another approach for identifying these critical points is by using energy methods as proposed by Murakami and Tanaka [1976] and Miyazaki [1986]; yet it is not considered here.

For completeness and clarity, the behaviour of the dome at three different times (namely: $t = 28$, $t = 150$, and $t = 180$ days) obtained with $\xi = 0.05$ is depicted in Figure 8. The behaviour at $t = 28$ days corresponds to the response immediately after the gradual loading, and the behaviours at $t = 150$ and

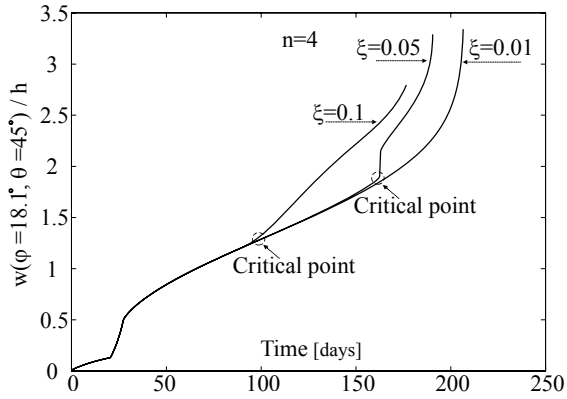

Figure 5. Nonaxisymmetric imperfection with $n = 4$ (scenario 2): variation in time of selected deflection with different imperfection amplitudes.

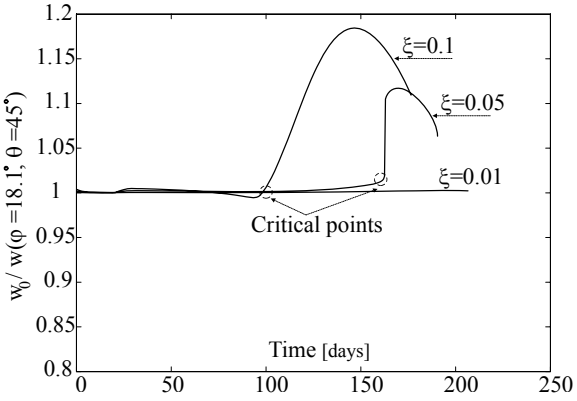

Figure 6. Nonaxisymmetric imperfection (scenario 2): ratio between the axisymmetric term and total solution.

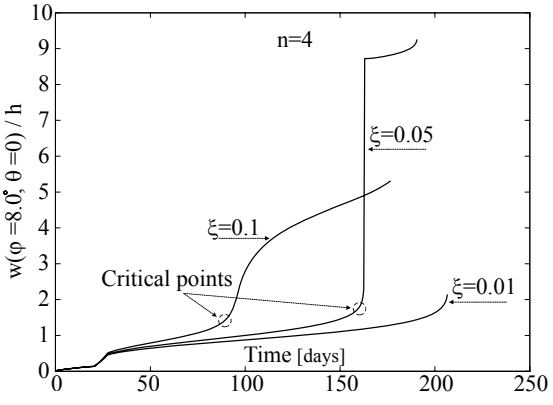

Figure 7. Nonaxisymmetric imperfection with $n = 4$ (scenario 2): variation in time of peak deflection with different imperfection amplitudes.

180 days correspond to the response before and after the critical point. Figure 8 shows that the time-dependent effects significantly increase and modify the distribution of the perpendicular deformations and internal forces. The distribution in the circumferential direction is governed by the characteristic circumferential wave number of the imposed imperfection, which equals 4. Figure 8b shows that at $t = 28$ days, the ratio between the deflection at any given circumferential angle θ to that at $\theta = 0$ is close to 1.0. However, this ratio decreases in time and becomes almost 0.05 at $t = 180$ days, which reflects the effect of the nonaxisymmetric harmonics on the overall response. It is also seen that the internal forces become relatively large at $t = 180$ days, and specifically, the circumferential forces change from compression to tension in some locations. These tension forces cause cracking and eventually initiate the failure of the dome. Finally, note that due to the geometric nonlinearity and the combined action of creep and shrinkage, and their interaction, the location of the peak response varies along the meridian (Figures 8a, 8c, and 8e). These effects highlight the need to use detailed theoretical models for the nonlinear long-term analysis of concrete domes.

The effect of the characteristic circumferential wave number n on the response of the dome is studied in Figure 9 for the nonaxisymmetric geometric imperfection given by (36) with $\xi = 0.05$. In order to approximately identify the ultimate time for creep buckling failure, the variation of the deflection at two critical locations is plotted. Figure 9a shows that with $n = 6$, a critical point develops at around $t = 65$ days compared to 162 days with $n = 4$, and Figure 9b shows that a critical point with $n = 5$ develops at $t = 130$ days. As discussed earlier, these critical points, which are associated with relatively large deformations, are considered as failure points in concrete structures, and so the long-term behaviour and ultimate time of shallow concrete domes are also affected by the characteristic wave number.

Third imperfection scenario: variable stiffness. Figure 10 shows the effect of sinusoidally varying stiffness according to (37). Different magnitudes of the imperfection parameter (ξ, the reduction factor of the membrane rigidity) and the circumferential wave number n are examined. The results show that relatively small reductions in the effective thickness of the dome and the corresponding membrane and bending rigidities significantly decrease the ultimate time for creep buckling of the dome. It is also seen that the characteristic circumferential wave number in this case significantly and nonlinearly affects the nonlinear creep behaviour of the dome. These effects play important roles in the structural behaviour of thin-walled concrete domes, and should be carefully considered in their design.

5. Conclusions

The creep buckling behaviour of thin-walled imperfect shallow concrete domes has been studied and some of the main aspects that characterize their behaviour have been revealed and clarified. This has been achieved by the development of a theoretical model for their nonlinear long-term analysis. The variational principle of virtual work and the principle of superposition, which accounts for the aging of the concrete material and the variation of stresses and geometry of the dome in time, have been used for the derivation of the governing equations. An incremental time-stepping approach has been used for the solution in time, while the truncated Fourier series and the multiple shooting method have been used for the solution in space allowing for different boundary conditions, loading schemes, and imperfection scenarios.

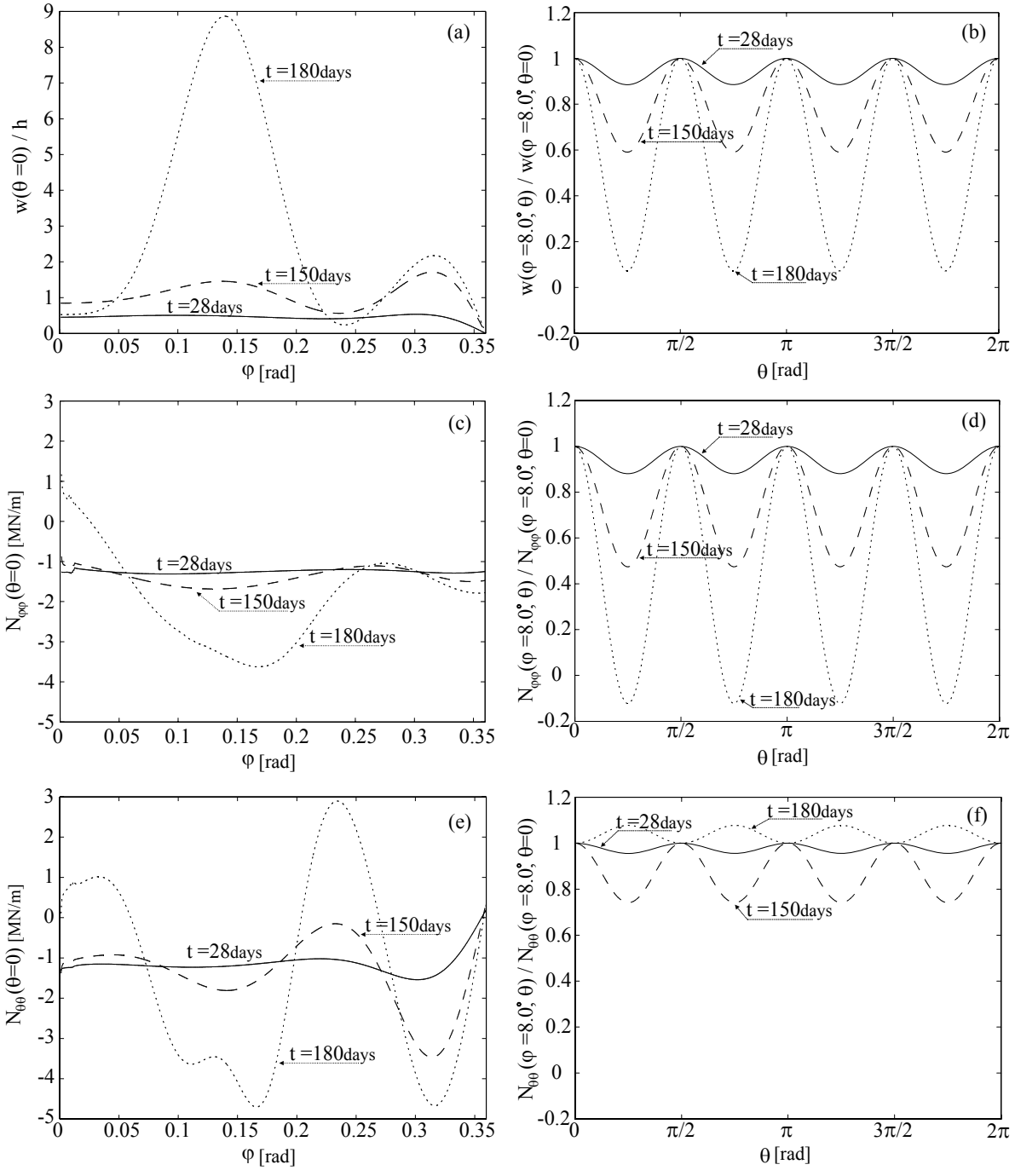

Figure 8. Structural response at three different times of a dome with nonaxisymmetric geometric imperfection ($\xi = 0.05$, $n = 4$): (a, b) perpendicular deformation; (c, d) radial force; (e, f) circumferential force. Solid line: $t = 28$ days; dashed line: $t = 150$ days; dotted line: $t = 180$ days.

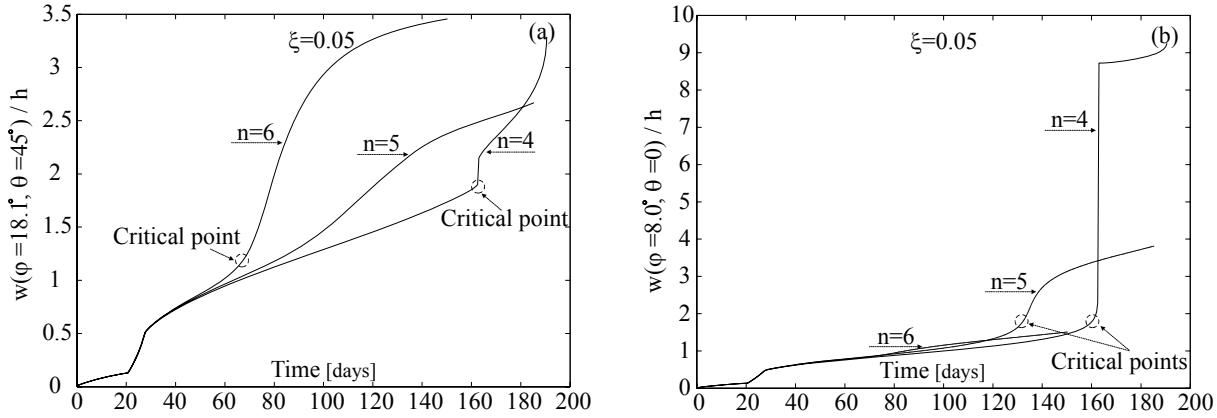

Figure 9. Behaviour in time under nonaxisymmetric imperfection (scenario 2) with $\xi = 0.05$ and different circumferential wave numbers: (a) deflection at $\varphi = 18.1°$ and $\theta = 45$; (b) deflection at $\varphi = 8.0°$ and $\theta = 0$.

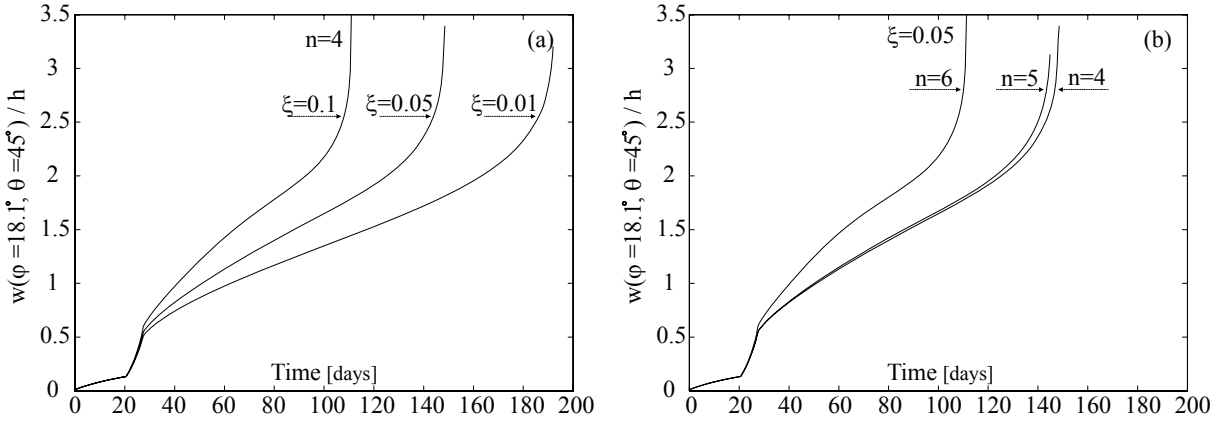

Figure 10. Varying stiffness imperfection (scenario 3): (a) variation in time of peak deflection with $n = 4$ and different imperfection amplitudes; (b) variation in time of peak deflection with $\xi = 0.05$ and different circumferential wave numbers.

Since the geometric imperfection in a dome to be constructed is not known at the design stage, both the form and the amplitude of the expected imperfection have been considered in the numerical study including an imperfection case that approximately simulates the effect of varying rigidities due to radial preloading shrinkage cracks or other construction inaccuracies, which are unique to domes made of concrete. It has been quantitatively shown that small departures from sphericity and the potential varying rigidities of the dome in the circumferential direction, significantly affect the long-term nonlinear behaviour and structural safety of shallow spherical concrete domes. Both the shape and amplitude of the imperfection have affected the behaviour and led to significant reductions in the ultimate time for creep buckling. Because in reality such imperfections cannot be avoided and are more prominent in concrete structures in general, and in curved concrete members in particular, a reliable prediction of the

imperfection effects is required. In addition, more imperfection scenarios than those examined in this paper should be considered for a detailed design of shallow concrete domes.

This paper contributes to the establishment of a foundation of theoretical knowledge required for long-term reliable analysis, effective design, and safe use of shallow concrete domes and general thin-walled concrete structures considering their potential imperfect shape. The results presented here show that the long-term effects of creep and shrinkage have a critical effect on the safety and the design life of shallow concrete domes. Finally, the modelling concepts and numerical tools and algorithms developed here can be further enhanced and generalized for the nonlinear long-term analysis of general thin-walled concrete structures, while the material nonlinearity and the development of a perturbation analysis for the characterization of bifurcation points are also considered for future research work.

References

[ACI 1982] ACI Committee 209, "Prediction of creep, shrinkage, and temperature effects in concrete structures", ACI Committee Report 209R-82, American Concrete Institute, Detroit, MI, 1982.

[Arbabi-Kanjoori and Leonard 1979] F. Arbabi-Kanjoori and J. Leonard, "Creep of non-symmetrically loaded shells of revolution", *Eng. Struct.* **1**:3 (1979), 145–152.

[Arnold et al. 1989] S. M. Arnold, D. N. Robinson, and A. F. Saleeb, "Creep buckling of cylindrical shell under variable loading", *J. Eng. Mech.* (*ASCE*) **115**:5 (1989), 1054–1074.

[AS 3600 2001] *Concrete structures*, 3rd ed., Australian Standard **AS 3600-2001**, The Association, Homebush, NSW, 2001.

[Bažant 1972] Z. P. Bažant, "Numerical determination of long-range stress history from strain history in concrete", *Mater. Struct.* **5**:3 (1972), 135–141.

[Bažant 1987] Z. P. Bažant, "Limitations of strain-hardening model for concrete creep", *Cem. Concr. Res.* **17**:3 (1987), 505–509.

[Bažant 1988] Z. P. Bažant, *Mathematical modeling of creep and shrinkage of concrete*, Wiley, New York, 1988.

[Bažant and Chern 1984] Z. P. Bažant and J.-C. Chern, "Rate-type concrete creep law with reduced time", *J. Eng. Mech.* (*ASCE*) **110**:3 (1984), 329–340.

[Billington 1982] D. P. Billington, *Thin shell concrete structures*, McGraw-Hill, New-York, 1982.

[Błachut and Galletly 1990] J. Błachut and G. D. Galletly, "Buckling strength of imperfect spherical caps: some remarks", *AIAA J.* **28**:7 (1990), 1317–1319.

[Błachut and Galletly 1995] J. Błachut and G. D. Galletly, "Buckling strength of imperfect steel hemispheres", *Thin-Walled Struct.* **23**:1–4 (1995), 1–20.

[Bockhold and Petryna 2008] J. Bockhold and Y. S. Petryna, "Creep influence on buckling resistance of reinforced concrete shells", *Comput. Struct.* **86**:7–8 (2008), 702–713.

[Bushnell 1976] D. Bushnell, "BOSOR5: program for buckling of elastic-plastic complex shells of revolution including large deflections and creep", *Comput. Struct.* **6**:3 (1976), 221–239.

[Bushnell 1977] D. Bushnell, "A strategy for the solution of problems involving large deflections, plasticity and creep", *Int. J. Numer. Methods Eng.* **11**:4 (1977), 683–708.

[Buyukozturk and Shareef 1985] O. Buyukozturk and S. S. Shareef, "Constitutive modeling of concrete in finite element analysis", *Comput. Struct.* **21**:3 (1985), 581–610.

[DPW NSW 1978] Department of Public Works, New South Wales, *Construction of Binishell reinforced concrete domes: New South Wales, Australia*, DPW, Sydney, 1978.

[Dulácska and Kollár 1995] E. Dulácska and L. Kollár, "Design procedure for the buckling analysis of reinforced concrete shells", *Thin-Walled Struct.* **23**:1–4 (1995), 313–321.

[Gilbert 1988] R. I. Gilbert, *Time effects in concrete structures*, Elsevier, Amsterdam, 1988.

[Gioncu 1979] V. Gioncu, *Thin reinforced concrete shells: special analysis problems*, Wiley, Chichester, 1979.

[Gould 1988] P. L. Gould, *Analysis of shells and plates*, Springer, New York, 1988.

[Grigolyuk and Lopanitsyn 2003] E. I. Grigolyuk and Y. A. Lopanitsyn, "The non-axisymmetric postbuckling behaviour of shallow spherical domes", *J. Appl. Math. Mech.* **67**:6 (2003), 809–818.

[Hamed et al. 2008] E. Hamed, M. A. Bradford, and R. I. Gilbert, "Effects of boundary conditions on the non-linear long-term behaviour of spherical shallow concrete domes", in *Proceedings of the 6th International Conference on Computation of Shell and Spatial Structures* (*IASS-IACM 2008*)*: Spanning nano to mega* (Ithaca, NY, 2008), edited by J. F. Abel and J. R. Cooke, Cornell University, Ithaca, NY, 2008. CD-ROM.

[Hamed et al. 2009a] E. Hamed, M. A. Bradford, and R. I. Gilbert, "Nonlinear time-dependent behaviour of spherical shallow concrete domes: shallowness effect", pp. 823–827 in *Futures in mechanics of structures and materials: proceedings of the 20th Australasian Conference on the Mechanics of Structures and Materials* (*ACMSM20*) (Toowoomba, 2008), edited by T. Aravinthan et al., CRC, Boca Raton, FL, 2009.

[Hamed et al. 2009b] E. Hamed, M. A. Bradford, and R. I. Gilbert, "Time-dependent and thermal behaviour of spherical shallow concrete domes", *Eng. Struct.* **31**:9 (2009), 1919–1929.

[Hamed et al. 2010] E. Hamed, M. A. Bradford, and R. I. Gilbert, "Nonlinear long-term behaviour of spherical shallow thin-walled concrete shells of revolution", *Int. J. Solids Struct.* **47**:2 (2010), 204–215.

[Hoff 1968] N. J. Hoff, "Axially symmetric creep buckling of circular cylindrical shells in axial compression", *J. Appl. Mech.* (*ASME*) **35**:3 (1968), 530–538.

[Hong and Teng 2002] T. Hong and J. G. Teng, "Non-linear analysis of shells of revolution under arbitrary loads", *Comput. Struct.* **80**:18–19 (2002), 1547–1568.

[Hong and Teng 2008] T. Hong and J. G. Teng, "Imperfection sensitivity and postbuckling analysis of elastic shells of revolution", *Thin-Walled Struct.* **46**:12 (2008), 1338–1350.

[Huang 1965] N. C. Huang, "Axisymmetrical creep buckling of clamped shallow spherical shells", *J. Appl. Mech.* (*ASME*) **32**:2 (1965), 323–330.

[Kao 1981] R. Kao, "Nonlinear creep buckling analysis of initially imperfect shallow spherical shells", *Comput. Struct.* **14**:1–2 (1981), 111–122.

[Litle et al. 1970] W. A. Litle, F. J. Forcier, and P. H. Griggs, "Can plastic models represent the buckling behavior of reinforced concrete shells?", pp. 265–288 in *Models for concrete structures*, ACI Special Publication **24**, American Concrete Institute, Detroit, MI, 1970.

[Marcinowski 2007] J. Marcinowski, "Stability of relatively deep segments of spherical shells loaded by external pressure", *Thin-Walled Struct.* **45**:10–11 (2007), 906–910.

[Minahen and Knauss 1993] T. M. Minahen and W. G. Knauss, "Creep buckling of viscoelastic structures", *Int. J. Solids Struct.* **30**:8 (1993), 1075–1092.

[Miyazaki 1986] N. Miyazaki, "On the finite element formulation of bifurcation mode of creep buckling of axisymmetric shells", *Comput. Struct.* **23**:3 (1986), 357–363.

[Miyazaki et al. 1991] N. Miyazaki, S. Hagihara, and T. Munakata, "Creep buckling under varying loads", *J. Pressure Vessel Technol.* (*ASME*) **113**:1 (1991), 41–45.

[Moncarz et al. 2007] P. D. Moncarz, M. Griffith, and P. Noakowski, "Collapse of a reinforced concrete dome in a wastewater treatment plant digester tank", *J. Perform. Constr. Facil.* (*ASCE*) **21**:1 (2007), 4–12.

[Muc 1992] A. Muc, "On the buckling of composite shells of revolution under external pressure", *Compos. Struct.* **21**:2 (1992), 107–119.

[Murakami and Tanaka 1976] S. Murakami and E. Tanaka, "On the creep buckling of circular cylindrical shells", *Int. J. Mech. Sci.* **18**:4 (1976), 185–194.

[Obrecht 1977] H. Obrecht, "Creep buckling and postbuckling of circular cylindrical shells under axial compression", *Int. J. Solids Struct.* **13**:4 (1977), 337—355.

[Reissner 1946] E. Reissner, "Stresses and small displacements of shallow spherical shells", *J. Math. Phys.* (*MIT*) **25** (1946), 80–85 and 279–300.

[Sheinman 1981] I. Sheinman, "Application of DSISR program to recessed shells of revolution", *Comput. Struct.* **14**:5–6 (1981), 361–368.

[Sheinman and Jabareen 2005] I. Sheinman and M. Jabareen, "Postbuckling of laminated cylindrical shells in different formulations", *AIAA J.* **43**:5 (2005), 1117–1123.

[Shi et al. 1970] J. J. J. Shi, C. D. Johnson, and N. R. Bauld, Jr., "Application of the variational theorem for creep of shallow spherical shells", *AIAA J.* **8**:3 (1970), 469–476.

[Stoer and Bulirsch 2002] J. Stoer and R. Bulirsch, *Introduction to numerical analysis*, 3rd ed., Texts in Applied Mathematics **12**, Springer, New York, 2002.

[Sundararajan and Noah 1997] P. Sundararajan and S. T. Noah, "Dynamics of forced nonlinear systems using shooting/arc-length continuation method: application to rotor systems", *J. Vib. Acoust.* (*ASME*) **119**:1 (1997), 9–20.

[Takeuchi et al. 2004] H. Takeuchi, S. Taketomi, S. Samukawa, and A. Nanni, "Renovation of concrete water tank in Chiba prefecture, Japan", *Pract. Period. Struct. Des. Constr.* **9**:4 (2004), 237–241.

[Teng and Hong 2006] J. G. Teng and T. Hong, "Postbuckling analysis of elastic shells of revolution considering mode switching and interaction", *Int. J. Solids Struct.* **43**:3–4 (2006), 551–568.

[Teng and Lou 1997] J. G. Teng and Y. F. Lou, "Post-collapse bifurcation analysis of shells of revolution by the accumulated arc-length method", *Int. J. Numer. Methods Eng.* **40**:13 (1997), 2369–2383.

[Teng and Rotter 1992] J. G. Teng and J. M. Rotter, "Geometrically and materially nonlinear analysis of reinforced concrete shells of revolution", *Comput. Struct.* **42**:3 (1992), 327–340.

[Teng and Song 2001] J. G. Teng and C. Y. Song, "Numerical models for nonlinear analysis of elastic shells with eigenmode-affine imperfections", *Int. J. Solids Struct.* **38**:18 (2001), 3263–3280.

[Vandepitte and Lagae 1986] D. Vandepitte and G. Lagae, "Buckling of spherical domes made of microconcrete and creep buckling of such domes under long-term loading inelastic behaviour of plates and shells", pp. 291–311 in *Inelastic behaviour of plates and shells: proceedings of IUTAM Symposium* (Rio de Janeiro, 1985), edited by L. Bavilacqua et al., Springer, Berlin, 1986.

[Wunderlich and Albertin 2002] W. Wunderlich and U. Albertin, "Buckling behaviour of imperfect spherical shells", *Int. J. Non-Linear Mech.* **37**:4–5 (2002), 589–604.

[Xirouchakis and Jones 1980] P. C. Xirouchakis and N. Jones, "Axisymmetric and bifurcation creep buckling of externally pressurised spherical shells", *Int. J. Solids Struct.* **16**:2 (1980), 131–148.

[Zarghamee and Heger 1983] M. S. Zarghamee and F. J. Heger, "Buckling of thin concrete domes", *ACI Struct. J.* **80**:6 (1983), 487–500.

Received 18 Mar 2009. Revised 22 Jun 2009. Accepted 3 Jul 2009.

EHAB HAMED: e.hamed@unsw.edu.au
Centre for Infrastructure Engineering and Safety, School of Civil and Environmental Engineering, The University of New South Wales, Sydney, NSW 2052, Australia

MARK A. BRADFORD: m.bradford@unsw.edu.au
Centre for Infrastructure Engineering and Safety, School of Civil and Environmental Engineering, The University of New South Wales, Sydney, NSW 2052, Australia

R. IAN GILBERT: I.Gilbert@unsw.edu.au
Centre for Infrastructure Engineering and Safety, School of Civil and Environmental Engineering, The University of New South Wales, Sydney, NSW 2052, Australia